中国光学 Chinese Optics 核心期刊

绿光波段60 pm超窄带滤光片的研制

王凯旋 陈刚 刘定权 马冲 张秋玉

Fabrication of an ultra-narrow band-pass filter with 60 pm bandwidth in green light band

WANG Kai-xuan, CHEN Gang, LIU Ding-quan, MA Chong, ZHANG Qiu-yu

引用本文:
王凯旋, 陈刚, 刘定权, 马冲, 张秋玉. 绿光波段60 pm超窄带滤光片的研制[J]. 中国光学, 2022, 15(1): 119-131. doi: 10.37188/CO.2021-0092
WANG Kai-xuan, CHEN Gang, LIU Ding-quan, MA Chong, ZHANG Qiu-yu. Fabrication of an ultra-narrow band-pass filter with 60 pm bandwidth in green light band[J]. *Chinese Optics*, 2022, 15(1): 119-131. doi: 10.37188/CO.2021-0092

在线阅读 View online: https://doi.org/10.37188/CO.2021-0092

文章编号 2095-1531(2022)01-0119-13

Fabrication of an ultra-narrow band-pass filter with 60 pm bandwidth in green light band

WANG Kai-xuan[1,2,3], CHEN Gang[1], LIU Ding-quan[1,2,3 *], MA Chong[1], ZHANG Qiu-yu[1,3]

(1. *Shanghai Institute of Technical Physics*, *Chinese Academy of Sciences*, *Shanghai* 200083, *China*;
2. *School of Physical Science and Technology*, *ShanghaiTech University*, *Shanghai* 200031, *China*;
3. *University of Chinese Academy of Sciences*, *Beijing* 100049, *China*)

* *Corresponding author*, *E-mail*: *dqliu@mail.sitp.ac.cn*

Abstract: Owing to the strong penetrating ability in the atmosphere, 532 nm-wavelength green laser has wide applications including free-space optical communications and laser three-dimensional mapping. A spectral filter, with a half-power bandwidth of less than 100 pm, is an important optical element to suppress the interference of background light. Therefore, an ultra-narrow band-pass filter based on optical interference film is designed and fabricated in this paper. The high and low refractive index film are made of tantalum pentoxide (Ta_2O_5) and silicon dioxide (SiO_2), respectively. The designed optical thin films are deposited on a fused quartz substrate by double-ion-beam sputtering deposition method. The transmission spectra of the filters are measured by a tunable laser and a power meter. The half-power bandwidths of the filters are (60±2) pm, and the transmittance reaches 62.6%.

Key words: optical thin film; thin film filter; picometer bandwidth; green light band; space laser mapping

绿光波段 60 pm 超窄带滤光片的研制

王凯旋[1,2,3], 陈 刚[1], 刘定权[1,2,3 *], 马 冲[1], 张秋玉[1,3]

(1. 中国科学院 上海技术物理研究所, 上海 200083;
2. 上海科技大学 物质学院, 上海 201210;
3. 中国科学院大学, 北京 100049)

摘要: 波长为 532 nm 的绿色激光在大气层中有较强的穿透能力, 可用于自由空间光通信和激光三维测绘, 为了抑制背景光的干扰, 需要半功率带宽小于 100 pm 的光谱滤波器。因此, 设计并研制了基于光学干涉薄膜的超窄带滤光片。将五氧化二钽(Ta_2O_5)和二氧化硅(SiO_2)分别作为高低折射率膜层材料, 将熔石英作为基片, 采用双离子束溅射沉积方法制备出所设计的光学薄膜。利用可调谐激光器和功率计测量滤光片的透射光谱, 其半功率带宽为(60±2) pm, 透过率达到 62.6%。

关 键 词: 光学薄膜; 薄膜滤光片; 皮米带宽; 绿光波段; 空间激光测绘

中图分类号: O484 **文献标志码:** A **doi:** 10.37188/CO.2021-0092

收稿日期: 2021-04-23; **修订日期:** 2021-05-21

基金项目: 上海市自然科学基金(No. 17ZR1434900)

Supported by Natural Science Foundation of Shanghai Municipality, China (No. 17ZR1434900)

1 Introduction

The green laser with 532 nm wavelength has strong penetrating ability in the atmosphere, and the corresponding light source and photoelectric receiver have stable performance. The laser with this wavelength has a good application prospect in laser lidar, free-space optical communications, space laser remote sensing, 3D mapping imaging and other fields[1-4]. In order to reduce the interference of background light, especially the strong influence of solar radiation, a spectral filter with passband width below 100 pm (i.e. 0.1 nm) is needed to suppress the background light[5]. For such a filter, the main filtering techniques that can be adopted include: acoustoptic modulation, atomic filtering, Fabry-Perot (F-P) etalon, thin film interference filtering, etc.[6-8].

For spaceborne optical instruments (especially those facing a deep space flight), reliability, high optical efficiency and light weight are the key factors to be considered, so the F-P etalon and thin film interference are the main technical options. E. Troupaki[5] et al. constructed a spectral filter by using the F-P etalon technique, and achieved 30 pm bandwidth spectral filtering on American ICESat-2 satellite for the elevation mapping of snow and ice, clouds and land. The instrument uses 6 laser beams for mapping. ICESat-2 is the only altitude-mapping satellite currently in use abroad. This kind of spectral filter has high requirements for temperature control. Moreover, it is difficult to arrange many spectral filters when quite a lot of laser beams are needed. In order to develop the space elevation mapping with more laser beams, we designed and fabricated a bandpass filter with a target bandwidth of 60 pm based on precision optical thin film.

2 Design and fabrication of film system

Several related subnano-level spectral filtering techniques are listed in Table 1, each of which has its own characteristics. In this paper, the spectral filtering technique based on thin film interference is adopted.

Tab. 1 Comparison of main filtering techniques for sub-nanometer spectrum in visible light band

表 1 可见光波段的主要亚纳米光谱滤波技术比较

Spectral filtering technique	Spectral fineness	Optical efficiency	Wave option	Structure	Stability
Acoustoptic modulation	1~0.01 nm	Medium	Fast modulated	Complex	Good
Atomic filtering	1~0.001 nm	High−low	Fixed, fewer options	Complex	Not bad
F-P etalon	1~0.002 nm	High	Fixed, more options	Somewhat complex	Good
Film interference	1~0.03 nm	High	Fixed, more options	Simple	Very good

2.1 Design of filtering film system

For the band-pass filter with very narrow half-power bandwidth, the F-P structure with a single resonator is adopted to form a filter with all-medium film layer considering the actual deposition error of each layer of film. Its waveform is comparable to that of a filter based on F-P etalon, and its spectrum rectangularity can be improved by increasing the interference order of spacer layer. Ta_2O_5 is selected as the high-index film layer and is applicable to ultra-narrow band-pass filters, such as the Dense Wavelength Division Multiplexing (DWDM) filter used in 4G and 5G optical communications, due to its excellent physical and chemical stability and transparency in near-ultraviolet, visible and short-wave infrared bands[9-11]. SiO_2 is selected as the low-index film layer, which has good transparency, high physical and chemical stability and good

thermal matching with the substrate made of fused quartz due to the sharing of the same material. Fused quartz (JGS-1, 4 mm thick) is selected as the substrate of the ultra-narrow band-pass filter due to its good thermal stability[12].

The filtering film system is designed as Sub./ (1H 1L)^{10} 1H 2L 1H (1L 1H) ^{10} 1L / Air, where H and L respectively represent the Ta_2O_5 and SiO_2 film layers with an optical thickness of 1/4 central wavelength, which is the laser wavelength of 532 nm. The low-index film layer 2L is designed as a spacer, since it has smaller linear expansion coefficient and refractive-index temperature coefficient, so has more stable filter spectrum compared with 2H spacer. Of course, this film system is also more sensitive to the incident angle. This is a Fabry-Perot structure with a single resonator, consisting entirely of dielectric films.

The passband width can be approximated by Equation (1)[13-14]:

$$2\Delta\lambda = \frac{4\lambda_0 n_{\mathrm{L}}^{2x-1} n_g}{m\pi n_{\mathrm{H}}^{2x}} \cdot \frac{n_{\mathrm{H}} - n_{\mathrm{L}}}{n_{\mathrm{H}} - n_{\mathrm{L}} + n_{\mathrm{L}}/m} \quad , \qquad (1)$$

where n_{H} and n_{L} are respectively the refractive indices of the high and low index film layers, n_g is the refractive index of the substrate (n_g =1.445), x is the number of the high-index film layers in the reflective film stack (x=11), λ_0 is the central wavelength (λ_0=532 nm), and m is the interference order of the filter (m = 1). At 532 nm wavelength, n_{H} and n_{L} are assumed to be 2.108 and 1.442[14] respectively for calculation, and the design value of half-power bandwidth is determined as 0.053 nm (53 pm). The bandwidth values calculated by Equation (1) are a series of separated values, among which 53 pm is the calculated value close to the target. Due to the influence of various technological factors in the actual film growth process and the existence of film-thickness monitoring error, the spectral passband will be widened to a certain extent.

Through "Film Wizard" film design software, the transmission spectrum curve of bandpass filter was obtained from the designed film system, as shown in Figure 1 (Color online). No antireflective film layer was designed on the other side of the substrate. When the light absorption of the film layer was not considered, the peak transmittance T_{P} reached 93% and the value of half-power bandwidth was 57 pm, it is little different from the result of Equation (1). When the light absorption of the film layer was considered and the extinction coefficients of the high and low index film layers (k_{H} = 1.5×10^{-5}, k_{L} =1.0×10^{-5}) were introduced[15], the peak transmittance T_{P} dropped to 74% and the value of half-power bandwidth increased to 65 pm. In the band with wavelengths less than 531.5 nm and larger than 532.5 nm, another filter with a wider passband would be used for spectral interception.

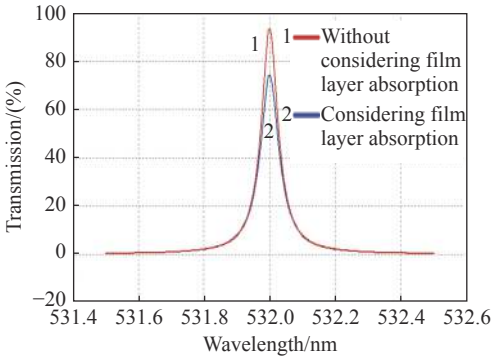

Fig. 1　Transmittance spectra of the designed ultra-narrow band-pass filter

图 1　设计的超窄带滤光片透射光谱

2.2　Film fabrication

For ultra-narrow band-pass filters, their optical films are mainly prepared with two techniques: (1) Ion Beam Assisted Deposition (IBAD); (2) Dual Ion Beam Sputtering (DIBS). Comparatively speaking, the film prepared by DIBS technique is denser, and the film and its components are more reliable and stable[16-19]. In this paper, the DIBS technique is used to prepare thin films. The layout and working diagram of the vacuum chamber of the coating equipment are shown in reference[15]. The sputtering ion source RF16 is the main ion source, generating the converging high-energy (Ar^+) ion beams to sputter the targets (Ta and SiO_2 targets). The (O^{2+} and Ar^+)

mixed ion beams generated by RF12 are used to bombard the film in growth to achieve full oxidation and dense growth of the film. The purity of the targets is ⩾99.99%. When the film was coated, the workpiece plate rotated at a high speed up to 800 r/min.

In the process of film deposition and growth, the Optical Monitoring System (OMS) emitted 532 nm light, which passed directly through a monitoring glass and was received by a detector. Then, an electrical signal was output from the detector to observe the change of light intensity. By substituting the filtering film system designed in Section 2.1 into the programming software "Film Maker", the intensity change and trend of the transmitted light signal can be calculated and displayed, as shown in Figure 2. As can be seen from Figure 2, the optical monitoring signal passing from the 14th layer to the 31st layer tends to be flat with a small variation, which will bring a large monitoring error. This requires improving the monitoring method by introducing a new monitoring glass when starting the film coating in an insensitive layer. The "OptiLayer" film software is used to analyze the sensitivity of each film layer. The sensitivity represents the degree of the influence of film layer error on filter spectrum. The lower the sensitivity, the less the influence of the error. The sensitivity of each film layer is given in Fig. 3. It can be seen that the sensitivity increases rapidly from the 13th layer. Therefore, it is necessary to increase the variation amplitude of optical monitoring signal in the film layers 14−31 in order to improve the monitoring accuracy of the film layers. Therefore, after the deposition of the 12th layer, a new monitoring glass should be used to monitor the deposition and growth of the next 32 (13th to 44th) layers, thereby effectively improving the monitoring accuracy of the sensitive film layers. The Fig. 4 shows the change of optical monitoring signal with the increase of film layers after introducing two monitoring samples. It can be seen that the amplitude of variation is significantly increased.

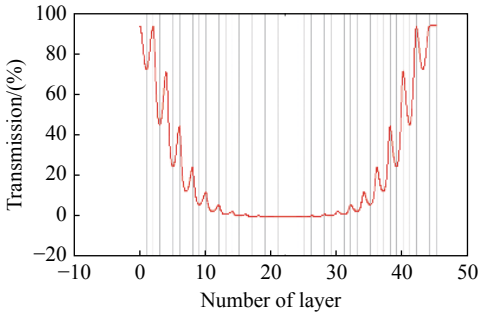

Fig. 2 Variation of the transmittance of optical signal as a function of the number of film layers

图 2 透射光控信号随膜层的变化

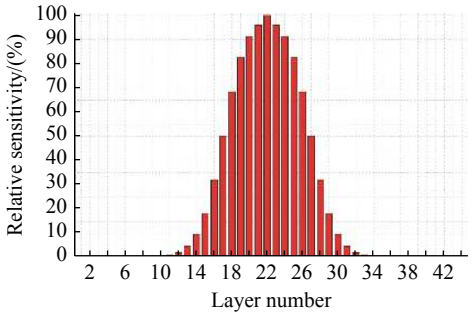

Fig. 3 Sensitivity of film layer error on filter spectrum in each layer

图 3 各个膜层误差对光谱影响的敏感度

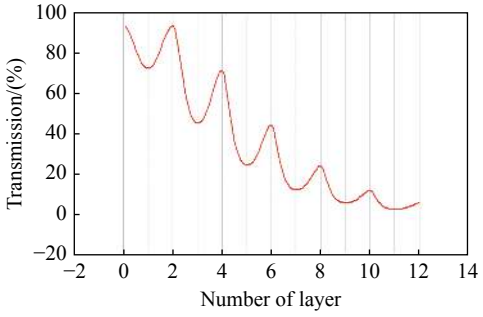

(a) 监控片 1

(a) Monitor plate 1

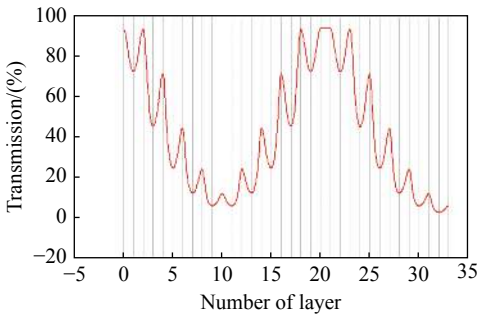

(b) 监控片 2

(b) Monitor plate 2

Fig. 4 Change of optical monitoring signal by using two separated monitor glass plates

图 4 分成两片监控后光控信号的变化

As can be seen from Fig. 4(b), the monitoring signal in the 20th layer on the monitoring glass 2 (the 32nd layer as a whole) has hardly changed, so the time monitoring method is adopted for this layer. This is a layer of SiO_2 film. The average deposition time of the 3 layers of SiO_2 film in front of this layer is calculated by the control computer, as the deposition time of this layer. As can be seen from Fig. 3, the sensitivity of this layer is relatively low. The use of this method can achieve higher monitoring accuracy.

2.3 Spectral measurement

For an ultra-narrow band-pass filter with the bandwidth less than 1 nm, its transmission spectrum measurement requires more accurate instrument. The spectral resolution of the instrument should be better than 1/10 of the filter bandwidth. The spectral integral energy penetrating the filter is very small, so the instrument needs very high detection sensitivity and is required to effectively control electrical measurement noise and background light interference.

The spectral measurement setup is shown in Fig. 5. The light source is a supercontinuum laser source with a spectral range of 400−2 000 nm, an output power of 8W, and a duty cycle of ⩾99%. The light is led out of the optical fiber and is vertically incident on the surface of the filter after collimation. After being collected, the light penetrating the filter is led by the optical fiber into a spectral analyzer (Yokogawa AQ6373B). The wavelength range of 531.5−532.5 nm is selected, and the sampling interval is 0.003 nm. The measured transmittance spectrum curve of the filter samples is shown in Fig. 6. Some fluctuations can be seen on both sides of the passband. These fluctuations are measurement noises and the curve is not smoothed.

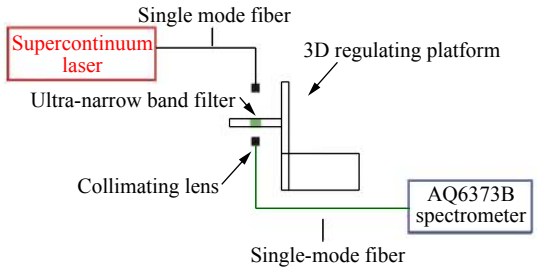

Fig. 5　Schematic diagram of the transmission spectrum measurement setup

图 5　透射光谱测量装置示意图

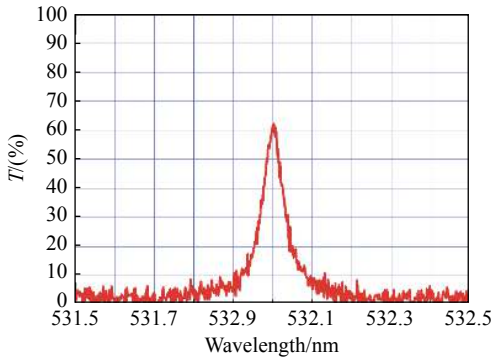

Fig. 6　Measured transmission spectrum of the ultra-narrow band-pass filter

图 6　测量的超窄带通滤光片的透射光谱

3 Analysis and discussion

3.1 Analysis of measurement spectrum

The comparison between Fig. 6 and Fig. 1 shows that the actually measured spectral passband is broadened and the peak transmittance is somewhat reduced. The specific data comparison is listed in Table 2.

Tab. 2　Data of measured and designed transmission spectrum

表 2　测量和设计的透射光谱数据

	Bandwidth (pm)	Peak transmittance (%)	Central wavelength (nm)
A. Design value (without absorption)	57	93.4	532.00
B. Design value (with absorption)	63	74.3	532.00
C. Measured value	62	62.6	532.009
D. Deviation value (from B)	−1	−11.7	+0.009

The film formed after actual deposition has a certain light absorption. In the process of deposition and growth, the optical control of film layer thickness always has some errors. Based on these two reasons, the actually measured spectrum is inconsistent with the designed spectrum.

(1) Effect of film absorption. The film absorption reduces the transmittance of optical energy, so that the transmittance of the spectral curve will de-

crease as a whole. As can be seen from Fig. 1 for this kind of ultra-narrow band filter, the peak transmittance is much smaller than that without film absorption, and the transmittance decreases a little at the wavelength far away from the peak wavelength. Thus the bandwidth corresponding to the half-peak value increases, and the *B* value is different from the *A* value, as shown in Table 2.

(2) Effect of film thickness control error. The control error of film thickness mainly includes the random error and the error caused by replacing the monitoring glass. The random error is usually very small, especially in the high-precision control system. Replacing the monitoring glass will change the initial growth state of the film, and thus will bring a certain error[20]. Due to the adoption of first-order vertical-transmission single-wavelength extremum monitoring method, the later deposited film layers can compensate for the error in the earlier film layers so that the optical thickness error of the whole film system will not be amplified. In order to investigate the influence of random error on the spectrum, the "OptiLayer" film software was used for simulation. An appropriate random error needs to be selected before simulation. Since the measured values of the filter bandwidth and central wavelength are not very different from the design values, the random error introduced should make the simulation results as close as possible to the design results, and should not be too large or too small. After several attempts, a random error of optical thickness equivalent to 10% of the passband width (i.e., 6 pm) was introduced to all layers. The simulation results are given in Fig. 7(a). Since the monitoring glass was replaced at the beginning of the 13th-layer plating, the effect of the random error of that layer on the spectrum needed to be investigated separately. For filters, the variations in passband width and central wavelength within 10% of the bandwidth are acceptable. After repeated attempts, the random error of each film layer was canceled, and a random error within 0.5% (i.e. 0.32 nm) of the optical thickness of the film layer was separately introduced into the 13th layer to obtain the simulation results shown in Fig. 7(b). By using the DIBS deposition technique, the film thickness accuracy can be controlled to 0.5%.

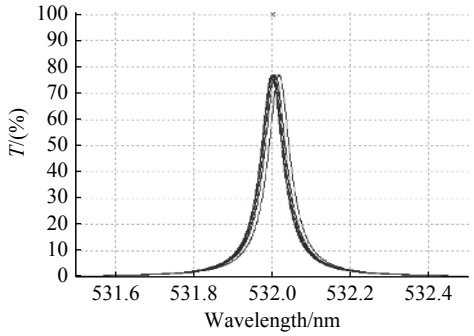

(a) 所有膜层引入通带宽度 10% 光学厚度的随机误差
(a) A random error of 10% of the optical thickness is introduced into all film layers

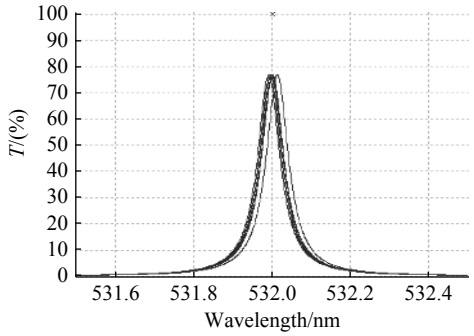

(b) 第 13 层引入不超过 0.5% 光学厚度的随机误差
(b) A random error within 0.5% of optical thickness is introduced into the 13th film layer

Fig. 7 Variation of spectral curves after randomly introducing the control errors

图 7 随机引入控制误差后的光谱曲线变化情况

As can be seen from Fig. 7, the introduction of these errors has little effect on the spectrum. The comparison with Fig. 6 indicates that the monitoring method used in this paper can control the random error within about 6 pm, thus forming a spectral passband with a width of 60 pm at 532 nm wavelength. The actual absorption of the film is larger than the set value, resulting in a further reduction of the peak transmittance. The bandwidth has no significant change, which is within the range of measurement error.

3.2 Influence of substrate

The material and surface quality of the substrate have a certain influence on the spectral char-

acteristics of this ultra-narrow band filter. The film deposition temperature is within the range of (100±5)℃, while the filter is usually used at normal temperature. Moreover, the environment may have temperature changes. Therefore, the linear expansion coefficient α of the film should be as close as possible to that of the substrate, and the refractive-index temperature coefficients (dn/dT) of the film and substrate should be as small as possible. Alternative substrate materials are given in Table 3, including Crystal Quartz (CQ), several types of glass, and sapphire (Al_2O_3).

Tab. 3　Optical and thermal properties of substrates and thin films in this study[12, 21-22]

表 3　基片和薄膜的光学和热特性[12, 21-22]

Materials	Refractive index, n@ 532nm,20~40 ℃	Refractive-index temperature coefficient, dn/dT (10^{-6}/℃)	Linear expansion coefficient, α (10^{-6}/℃) @0~100 ℃
Crystal Quartz (CQ)	1.55	5.2	13.4
Fused quartz (JGS-1)	1.46	10.0	0.55
Glass ceramics (Zerodur)	1.54	14.3	0.05
Glass (K9, BK7)	1.52	3.0	7.4
Sapphire (Al_2O_3)	1.77	13.1	6.7
SiO_2 film	1.44	9.0	0.55
Ta_2O_5 film	2.11	20.0	1.1

The CQ and sapphire (Al_2O_3) given in Table 3 have birefringence (but the data in Table 3 is for ordinary light (O light)) and a large linear expansion coefficient, so they were not selected in this study. Glass ceramics was also not selected due to its high refractive-index temperature coefficient. Optical glass (K9, BK7, etc.) is usually doped with some substances containing heavy metals, and exhibits a transmittance decrease under space irradiation, which has been confirmed in our previous experimental studies. Part of the data is from Schott's website. In this study, the JGS-1 fused quartz from China was selected as the substrate material.

The surface quality of the substrate also affects the spectral performance of the filter. If the surface is not smooth enough, a thin transition layer with an uncertain refractive index will be formed at the interface between the film and the substrate, as shown in Fig. 8, where $d_{s\text{-}f}$ is the geometric thickness of the transition layer. The refractive index $n_{s\text{-}f}$ of the transition layer is determined by Equation (2),

$$n_{s-f} = \rho_s n_s + (1-\rho_s) n_f \quad , \qquad (2)$$

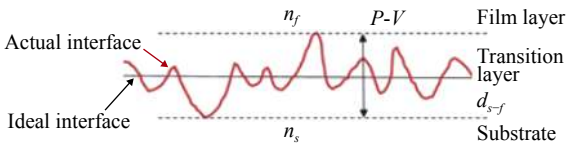

Fig. 8　Schematic diagram of the boundary between rough substrate surface and thin film

图 8　粗糙基片表面与薄膜分界示意图

where ρ_s is the volume proportion of the substrate material in the transition layer, n_s and n_f are the refractive index of the substrate and that of the first layer respectively. The optical thickness deviation caused by the transition layer can be given by Equation (3),

$$\Delta d = (n_{s-f} - n_f) d_{s-f} \quad . \qquad (3)$$

It can be seen that a rougher surface has a larger Δd value accordingly.

In this study, Δd should not be larger than 6 pm (10% of the bandwidth). Assuming the volume proportion ρ_s of 0.5 and the first layer of Ta_2O_5 and considering the film layer sensitivity shown in Fig. 4, the roughness P-V of the substrate surface should be less than 2 nm, so the surface is an ultra-

smooth surface.

3.3 Spectrum stability

The spectral measurement of the filter samples was made one month after the completion of cutting. The samples with qualified spectra were selected as products and applied in the laser mapping system. After one month of aging, the stress in the film has been released, the film system tends to be stable. The optical stability of the spacer layer 2L has the greatest influence on the spectrum, while the influence of other layers is relatively small. The spacer layer is made of the same material as the substrate. Under temperature control, small temperature changes will not generate new stresses. The change of the optical properties of the film with temperature will lead to spectral shift, which can be approximated by Equation (4) [12]:

$$\frac{\Delta\lambda}{\lambda_0}=\frac{\lambda_T-\lambda_0}{\lambda_0}=\frac{4}{\lambda_0}\left[\frac{P(n_H^T d_H^T)+Q(n_L^T d_L^T)}{P+Q}\right]-1 \quad , \tag{4}$$

where λ_0 is the preset central wavelength, and λ_T is the central wavelength at the temperature T; P is the number of cycles in the reflector film layers, P=11; Q is the order of the spacer layer, Q=1; $n_H^T d_H^T$ is the optical thickness of the high-index layer H at the temperature T, and $n_L^T d_L^T$ is the optical thickness of the low-index layer L at the temperature T.

By substituting the film system parameters of the filter into Equation (4), the change of its transmission spectrum with temperature was determined. The spectral drift is about 54 pm at the temperature change of 10℃, about 16 pm at the temperature change of 3℃, and about 2 pm at the temperature change of 2℃. In the actual optical system where the filter is applied, the temperature control condition is set to ±2℃. The filter behaves stably during the actual laser mapping process in space.

4 Conclusion

By using Ta_2O_5 and SiO_2 as high and low refractive index film materials respectively and fused quartz as the substrate, we prepared an ultra-narrow band filter with a half-power bandwidth of (60±2) pm, a central wavelength of 532.0 nm and a peak transmittance of 62.6% through DIBS deposition. When the insensitive film layers were deposited, the monitoring glass was switched, the accumulation amplification of errors were effectively controlled by using two monitoring glass plates one after another and first-order transmission extremum monitoring method. Finally, an ultra-narrow band filter with a measured half-power bandwidth of about 60 pm was obtained.

——中文对照版——

1 引 言

波长为 532 nm 的绿色激光在大气层中具有很好的穿透能力，相应的光源和光电接收器的性能稳定。该波长的激光在激光雷达、自由空间光通信、空间激光遥感和三维测绘成像等方面有着良好的应用前景[1-4]。为了减少背景光干扰，特别是太阳辐射的强烈影响，需要利用通带宽度在 100 pm（即 0.1 nm）以下的光谱滤波器来抑制背景光[5]。对于通带宽度小于 0.1 nm 的光谱滤波要求，可采用的主要技术方式有：声光调制技术、原子滤波技术、法布里-珀罗 (F-P) 标准具方式和薄膜干涉滤光技术等[6-8]。

对于空间光学仪器（特别是需要经历深空飞行的仪器），可靠性好、光学效率高和结构轻巧是需要重点考虑的因素，F-P 标准具和薄膜干涉技术成为可选的主要技术方式。E. Troupaki[5] 等用 F-P 标准具构建了光谱滤波组件，用于美国针对冰雪、云层和陆地进行高程测绘的 ICESat-2 卫星上，实现了 30 pm 带宽的光谱滤波，仪器用 6 束激光进行测绘。ICESat-2 卫星是目前国外唯一正在使用中的高程测绘卫星。这种光谱滤波组件对温度控制要求较高，在需要较多激光波束时难以合

理布局众多光谱滤波组件。为了发展更多激光波束的空间高程测绘, 以精密光学薄膜为基础, 设计制作了目标带宽为 60 pm 的带通滤光片。

2　膜系设计与制备

几种相关的亚纳米光谱滤波技术各有特点(见表 1), 本文采用薄膜干涉光谱滤波技术。

2.1　滤光膜系设计

对于半功率带宽非常窄的超窄带滤光片, 考虑各层薄膜在实际沉积时存在的误差, 采用单个谐振腔的 F-P 结构, 形成全介质膜层的滤光片。其波形与采用 F-P 标准具得到的光谱波形相当, 还可以用增加间隔层干涉级次的方法提升光谱的矩形程度。选用 Ta_2O_5 作为高折射率膜层, 它在近紫外、可见光和短波红外波段具有非常好的物理化学稳定性和透明性[9-11], 适合制作超窄带滤光片, 如 4G 和 5G 光通信中使用的密集波分复用滤波器(DWDM)。本文选用 SiO_2 作为低折射率膜层, SiO_2 具有良好的透明性和物理化学稳定性, 与基片熔融石英材质相同, 有良好的热匹配性。选用熔融石英作为滤光片基片, 其热稳定性好, 适合用作超窄带滤光片的基片[12], 基片采用厚度为 4 mm 的 JGS-1 熔融石英。

滤光膜系设计为: Sub./ (1H 1L)^{10} 1H 2L 1H (1L 1H) ^{10} 1L / Air。其中, H 和 L 分别表示光学厚度为 1/4 中心波长的 Ta_2O_5 和 SiO_2 膜层, 中心波长就是 532 nm 激光波长。将低折射率膜层 2L 设计为间隔层, 比起 2H 作为间隔层, 它的线膨胀系数和折射率温度系数更小一些, 滤光片的光谱也会更稳定一些。当然, 这种膜系对入射光线的角度也会敏感一些。这是单个谐振腔的 F-P 结构, 其完全由介质薄膜构成。

通带宽度计算, 可以由公式 (1) 得到近似值[13-14],

$$2\Delta\lambda = \frac{4\lambda_0 n_L^{2x-1} n_g}{m\pi n_H^{2x}} \cdot \frac{n_H - n_L}{n_H - n_L + n_L/m} \quad , \qquad (1)$$

其中, n_H和n_L分别为高低折射率膜层的折射率, n_g为基片的折射率(取值 1.445), x 为反射膜堆内高折射率膜层数(取值 11), λ_0为中心波长(取值 532 nm), m 为滤光片的干涉级次(m = 1)。在波长 532 nm 处, n_H和n_L分别取为 2.108 和 1.442[14] 进行计算, 得到半功率带宽的设计值为 0.053 nm (即 53 pm)。利用公式(1)计算得到的带宽值是一系列分离的数值, 53 pm 是接近目标的计算值。由于在实际薄膜生长的工艺过程中存在多种工艺因素的影响, 还存在膜层的厚度监控误差, 光谱通带会有一定程度的展宽。

将设计膜系代入 Film Wizard 光学薄膜设计软件, 得到带通滤光片的透射光谱曲线, 在图 1 (彩图见期刊电子版)中给出, 在基片另一面没有设计减反射膜层。在不考虑膜层光吸收的情况下, 峰值透过率T_p达到 93%, 半功率带宽的数值为 57 pm, 与式(1)差异不大; 在考虑膜层光吸收的情况下, 引入高低折射率膜层消光系数[15]: k_H=1.5×10^{-5} 和k_L=1.0×10^{-5}, 峰值透过率T_p降低到 74%, 半功率带宽的数值增加到 65 pm。在波长小于 531.5 nm 和大于 532.5 nm的区域, 将由另外的通带较宽的滤光片进行光谱拦截。

2.2　薄膜制备

对于超窄带滤光片, 光学薄膜的制备技术主要有两种: (1)离子束辅助沉积技术(Ion Beam Assisted Deposition, IBAD); (2)双离子束溅射技术(Dual Ion Beam Sputtering, DIBS)。相对而言, DIBS 技术制备的薄膜更加密实, 薄膜和元件的可靠性和稳定性也更好[16-19]。本文采用 DIBS 技术制备薄膜, 镀膜设备真空室内的布局和工作示意图见文献 [15]。其中溅射离子源 RF16 为主离子源, 它产生的高能会聚(Ar^+)离子束用于溅射靶材料(Ta 和 SiO_2 靶); 辅助轰击离子源 RF12 产生的(O^{2+}和 Ar^+)混合离子束对生长中的膜层进行轰击, 实现膜层的充分氧化和致密生长。靶材的纯度≥99.99%, 镀膜时工件盘高速转动, 转速达到 800 r/min。

在薄膜沉积生长过程中, 光学监控系统(OMS)发出 532 nm 波长的光直接穿过监控片, 被探测器接收后输出电信号, 用于观测光强度的变化。将前面 2.1 节中设计的滤光膜系代入编制软件 Film Maker 中, 可以计算并显示出透射光信号的强弱变化和走势, 如图 2 所示。从图 2 可以看出, 从第 14 层到第 31 层光学监控的信号趋于平坦, 变化幅度很小, 这样会给监控带来较大误差。因此, 需要改进监控方式, 在一个不敏感层开始镀膜时切入一个新的监控片。用 OptiLayer 光学薄膜软件分析了各个膜层的敏感度, 敏感度表

示该膜层误差对滤光片光谱的影响程度，敏感度越低则误差的影响越小。图 3 中给出了各个膜层的敏感度，可以看出从第 13 层开始敏感度迅速增大。所以，必须提高第 14 到 31 层薄膜光控信号的变化幅度，才能提升膜层的监控精度。因此，在第 12 层薄膜沉积完成后，更换一个新的监控片来监控后面 32 层（第 13 到 44 层）薄膜的沉积生长，以有效提升敏感膜层的监控精度。图 4给出了采用两个监控样品后，光学监控信号随膜层的变化情况，可见变化幅度明显提升。

从图 4(b)可以看到，监控片 2 上的第 20 层（总第 32 层）的监控信号几乎没有变化，对该层采用时间监控方法。这是一层 SiO_2 薄膜，由控制计算机计算出它前面 3 层 SiO_2 薄膜沉积的平均时间，作为该层薄膜的沉积时间。从图 3 可以看到，该层薄膜的敏感度是比较低的。采用这样的方法总体可以得到更高的监控精度。

2.3 光谱测量

带宽小于 1 nm 的超窄带滤光片的透射光谱测量需要更加精确的光谱测量仪器。仪器的光谱分辨能力应该优于滤光片带宽的 1/10；能够透过滤光片的光谱积分能量很小，仪器需要很高的探测灵敏度，同时能够有效控制测量电噪声和背景光干扰。

光谱测量装置如图 5 所示。光源选用超连续谱的激光光源，光谱范围为 400~2 000 nm，输出功率为 8 W，占空比≥99%；光线由光纤导出，准直后垂直入射滤光片表面；透过滤光片的光线被收集后由光纤导入光谱分析仪器（日本横河公司生产的 AQ6373B 光谱分析仪），选定 531.5~532.5 nm 波长，采样间隔为 0.003 nm。图 6 是测量得到的滤光片样品的透射率光谱曲线，在通带的两侧看到一些波动，这些波动是测量噪声，曲线没有经过平滑处理。

3 分析和讨论

3.1 测量光谱分析

对比图 6 和图 1 可以看出，实际测得的光谱通带有所展宽，峰值透过率也有所降低，具体数据对比见表 2。

实际沉积制成的薄膜对光有一定的吸收；在沉积生长过程中，膜层的光学厚度控制也总是存在一些误差。基于这两方面原因，造成了实际测量光谱与设计光谱不一致。

（1）膜层吸收的影响。膜层的吸收会减少透过的光学能量，使得光谱曲线的透过率整体下降。从图 1 可以看出，对于这种超窄带滤光片，峰值透过率下降较多，离峰值波长较远处下降较少，这就使得半峰值对应的带宽增大，出现了表 2 中 B 值和 A 值的差别。

（2）膜厚控制误差的影响。膜层厚度的控制误差主要来自随机误差和更换监控片带来的误差，随机误差通常很小，特别在高精度控制系统中，更换监控片改变了薄膜的初始生长状态，会带来一定的误差[20]。由于采用了 1 级次的垂直透射式单波长极值监控方法，后续沉积的膜层对前面制成的膜层有误差补偿作用，可以使得整个膜系的光学厚度误差不被放大。

为了考察随机误差对光谱的影响，用 OptiLayer 光学薄膜软件进行模拟。在进行模拟之前需要选择合适的随机误差。由于滤光片的带宽和中心波长的实测值与设计值差距不大，因此引入的随机误差应使模拟结果尽量接近设计结果，不宜过大或过小。在进行多次尝试后，引入了光学厚度相当于通带宽度 10%（即 6 pm）的随机误差到所有膜层，并给出了模拟结果（图 7(a)）。由于在镀制第 13 层薄膜开始时更换了监控片，所以需要单独考察该层的随机误差对光谱的影响。对于滤光片而言，通带宽度和中心波长的变化在带宽的 10% 以内是可以接受的。同样进行多次尝试后，取消各个膜层的随机误差，再单独引入 0.5% 光学厚度（即 0.32 nm）以内的随机误差到第 13 层薄膜中，并给出了模拟结果（图 7(b)）。对于用双离子束溅射薄膜沉积技术而言，膜厚精度控制到 0.5% 是可以实现的。

从图 7 可以看出，这些误差的引入对光谱的影响不大。对比图 6 可知，本文所用的监控方法可以把随机误差控制在约 6 pm 以内，因此能在 532 nm 波长处形成宽度为 60 pm 的光谱通带。薄膜的实际吸收能量比设定值要大一些，导致峰值透过率进一步降低，而带宽没有明显变化，变化量在测量误差范围内。

3.2 基片的影响

基片材质和表面质量对超窄带滤光片的光谱

特性有一定的影响。薄膜沉积温度在(100±5)℃范围,滤光片通常在常温环境中使用,考虑到使用环境可能的温度变化,薄膜和基片的线膨胀系数应尽可能接近,薄膜和基片材料的折射率温度系数 dn/dT 应尽量小。可供选择的基片材料在表 3 中给出,这些材料是石英晶体(Crystal Quartz, shoux, CQ)、几种玻璃和蓝宝石(Al_2O_3)。

表 3 中,石英晶体(CQ)和蓝宝石(Al_2O_3)有双折射现象,表 3 中数据选用的是寻常光(O 光)的数据,它们的线膨胀系数也较大,故在此研究中没有选用。微晶玻璃的折射率温度系数较高,也没有选用,光学玻璃(K9、BK7 等)中通常掺杂了一些含有重金属的物质,空间辐照条件下其透过率会下降,本课题组以前的研究已经证实。部分数据来源于德国 Schott 公司网页。本研究选择中国牌号的 JGS-1 熔融石英作为基片材料。

基片的表面质量也会影响滤光片的光谱性能。不够光滑的表面,在薄膜与基片的界面处会形成一层折射率不确定的过渡薄层,如图 8 所示。其中 $d_{s\text{-}f}$ 是过渡层的几何厚度。这个过渡层的折射率 $n_{s\text{-}f}$ 由式(2)决定:

$$n_{s-f} = \rho_s n_s + (1-\rho_s) n_f \quad , \tag{2}$$

其中 ρ_s 是基片材料在过渡层的体积占比,n_s 和 n_f 分别是基片的折射率和第 1 层薄膜的折射率。由过渡层引起的光学厚度偏差可以由式(3)给出:

$$\Delta d = (n_{s-f} - n_f) d_{s-f} \quad , \tag{3}$$

可以看出,粗糙表面对应的 Δd 值也较大。在本研究工作中,Δd 应该不大于 6 pm(带宽的 10%),按照 ρ_s 取 0.5 和第 1 层用 Ta_2O_5 薄膜来计算,结合图 3 考虑到膜层的敏感度,基片表面的粗糙度 P-V 值应该小于 2 nm,属于超光滑表面。

3.3　光谱的稳定性

滤光片样品的光谱测量是在切割完成一个月后进行的,筛选出光谱合格的样品作为产品应用在激光测绘系统中。经过一个月的老化,薄膜中的应力已经释放,薄膜体系趋于稳定。对光谱影响最大的是间隔层 2L 的光学稳定性,其他膜层的影响相对小一些。间隔层与基片的材质相同,在温控条件下,小的温度变化不会产生新的应力。膜层光学特性随温度的变化会导致光谱的移动。光谱的移动量近似得[12]:

$$\frac{\Delta\lambda}{\lambda_0} = \frac{\lambda_T - \lambda_0}{\lambda_0} = \frac{4}{\lambda_0}\left[\frac{P(n_H^T d_H^T) + Q(n_L^T d_L^T)}{P+Q}\right] - 1 \quad , \tag{4}$$

其中 λ_0 是设定中心波长,λ_T 是 T 温度下的中心波长;P 是反射板膜层的周期数,这里取 11;Q 是间隔层的级次,这里取 1;$n_H^T d_H^T$ 是 T 温度下高折射率膜层 H 层的光学厚度,$n_L^T d_L^T$ 是 T 温度下低折射率膜层 L 层的光学厚度。

将滤光片膜系参数带入公式(4),计算得到其透射光谱随温度变化的情况,即温度变化 10 ℃时光谱漂移约 54 pm,温度变化 3 ℃时光谱漂移约为 16 pm,温度变化 2 ℃时光谱漂移约为 2 pm。滤光片的实际应用光学系统,温控条件设置为±2℃,滤光片在空间实际激光测绘过程中表现稳定。

4　结　论

采用 Ta_2O_5 和 SiO_2 分别作为高低折射率膜层材料,熔石英为基片,利用双离子束溅射沉积方法制备了半功率带宽为(60±2) pm 超窄带滤光片,其中心波长为 532.0 nm,峰值透过率达到 62.6%。在不敏感膜层沉积时切换监控片,依次用 2 个监控片和 1 级次透射极值监控的方法,有效控制了误差的影响和积累放大,实测得到半功率带宽约为 60 pm 的超窄带滤光片。

References:

[1] YU A W, STEPHEN M A, LI S X, *et al*.. Space laser transmitter development for ICESat-2 mission[J]. *Proceedings of SPIE*, 2010, 7578: 757809.

[2] SAWRUK N W, STEPHEN M A, LITVINOVITCH S, *et al*.. Space qualified laser transmitter for NASA's ICESat-2 mission[J]. *Proceedings of SPIE*, 2013, 8599: 85990O.

[3] 高世杰, 吴佳彬, 刘永凯, 等. 微小卫星激光通信系统发展现状与趋势[J]. 中国光学, 2020, 13(6): 1171-1181.
GAO SH J, WU J B, LIU Y K, *et al*.. Development status and trend of micro-satellite laser communication systems[J]. *Chinese Optics*, 2020, 13(6): 1171-1181. (in Chinese)

[4] 董全睿, 陈涛, 高世杰, 等. 星载激光通信技术研究进展[J]. 中国光学, 2019, 12(6): 1260-1270.
DONG Q R, CHEN T, GAO SH J, *et al*.. Progress of research on satellite-borne laser communication technology[J]. *Chinese Optics*, 2019, 12(6): 1260-1270. (in Chinese)

[5] TROUPAKI E, DENNY Z H, WU S, *et al*.. Space qualification of the optical filter assemblies for the ICESat-2/ATLAS instrument[J]. *Proceedings of SPIE*, 2015, 9346: 93460H.

[6] 王建宇, 舒嵘, 刘银年, 等. 成像光谱技术导论[M]. 北京: 科学出版社, 2011: 90-110.
WANG J Y, SHU R, LIU Y N, *et al*.. *Introduction to Imaging Spectroscopy*[M]. Beijing: Science Press, 2011: 90-110. (in Chinese)

[7] HAN F, LIU H J, SUN D S, *et al*.. An ultra-narrow bandwidth filter for daytime wind measurement of direct detection Rayleigh lidar[J]. *Current Optics and Photonics*, 2020, 4(1): 69-80.

[8] GAYEN S K, BILLMERS R I, CONTARINO V M, *et al*.. Induced-dichroism-excited atomic line filter at 532 nm[J]. *Optics Letters*, 1995, 20(12): 1427-1429.

[9] XU CH, XIAO O L, MA J Y, *et al*.. High temperature annealing effect on structure, optical property and laser-induced damage threshold of Ta_2O_5 films[J]. *Applied Surface Science*, 2008, 254(20): 6554-6559.

[10] ZHAO Q, PU Y T, HAO L, *et al*.. Residual stress and laser-induced damage of ion-beam sputtered Ta_2O_5/SiO_2 mixture coatings[J]. *Thin Solid Films*, 2015, 592: 221-224.

[11] LV Q P, HUANG M L, ZHANG SH Q, *et al*.. Effects of annealing on residual stress in Ta_2O_5 films deposited by dual ion beam sputtering[J]. *Coatings*, 2018, 8(4): 150.

[12] KIM S H, HWANGBO C K. Derivation of the center-wavelength shift of narrow-bandpass filters under temperature change[J]. *Optics Express*, 2004, 12(23): 5634-5639.

[13] 唐晋发, 顾培夫, 刘旭, 等. 现代光学薄膜技术[M]. 杭州: 浙江大学出版社, 2006: 144-146.
TANG J F, GU P F, LIU X, *et al*.. *Modern Optical Thin Film Technology*[M]. Hangzhou: Zhejiang University Press, 2006: 144-146. (in Chinese)

[14] MACLEOD H A. *Thin-Film Optical Filters*[M]. Boca Raton: Taylor & Francis, 2010: 310-313.

[15] 陈刚. 几种金属氧化物薄膜的近红外光学性能和用于空间遥感的窄带通滤光片研究[D]. 上海: 中国科学院上海技术物理研究所, 2020: 56-68.
CHEN G. Research on the near infrared optical properties of several metal oxide thin films and narrow bandpass filters for space remote sensing[D]. Shanghai: Shanghai Institute of Technical Physics Chinese Academy of Sciences, 2020: 56-68. (in Chinese)

[16] CHANELIERE C, AUTRAN J L, DEVINE R A B, *et al*.. Tantalum pentoxide (Ta_2O_5) thin films for advanced dielectric applications[J]. *Materials Science and Engineering*: *R*: *Reports*, 1998, 22(6): 269-322.

[17] 袁文佳, 沈伟东, 郑晓雯, 等. 离子束溅射制备Nb_2O_5、Ta_2O_5和SiO_2薄膜的光学、力学特性和微结构 [J]. 光学学报, 2017, 37(12): 1231001.
YUAN W J, SHEN W D, ZHENG X W, *et al*.. Optical and mechanical properties and microstructures of Nb_2O_5, Ta_2O_5 and SiO_2 thin films prepared by ion beam sputtering[J]. *Acta Optica Sinica*, 2017, 37(12): 1231001. (in Chinese)

[18] 姜玉刚, 刘华松, 陈丹, 等. 基于离子束溅射Ta_2O_5薄膜的紫外吸收膜技术 [J]. 光学 精密工程, 2019, 27(3): 527-532.
JIANG Y G, LIU H S, CHEN D, *et al*.. Ultraviolet absorption film technology based on ion beam sputtering Ta_2O_5 thin films[J]. *Optics and Precision Engineering*, 2019, 27(3): 527-532. (in Chinese)

[19] 尚鹏, 熊胜明, 李凌辉, 等. 光谱法确定离子束溅射Ta_2O_5/SiO_2薄膜的光学常数及其性能 [J]. 光学学报, 2014, 34(5): 0531002.
SHANG P, XIONG SH M, LI L H, *et al*.. Optical constants and properties of dual-ion-beam sputtering Ta_2O_5/SiO_2 thin film by spectroscopy[J]. *Acta Optica Sinica*, 2014, 34(5): 0531002. (in Chinese)

[20] WU Q D. Nucleation and growth of vapor phase deposition on solid surfaces[J]. *Vacuum*, 1990, 41(4-6): 1431-1433.

[21] WAKAKI M, KUDO K, SHIBUYA T. *Physical Properties and Data of Optical Materials*[M]. Boca Raton: CRC Press, 2007: 301-330.

[22] 朱绪丹, 张荣君, 郑玉祥, 等. 椭圆偏振光谱测量技术及其在薄膜材料研究中的应用[J]. 中国光学, 2019, 12(6): 1195-1234.

ZHU X D, ZHANG R J, ZHENG Y X, *et al*.. Spectroscopic ellipsometry and its applications in the study of thin film materials[J]. *Chinese Optics*, 2019, 12(6): 1195-1234. (in Chinese)

Author Biographics:

Wang Kai-xuan (1992—), male, born in Bozhou, Anhui Province. Doctor. He received his Bachelor's degree from Beijing University of Aeronautics and Astronautics in 2013. Now he mainly engages in the research of optical thin film materials and devices. E-mail: wangkx@shanghaitech.edu.cn

王凯旋(1992—),男,安徽亳州人,博士研究生,2013 年于北京航空航天大学获得学士学位,主要从事光学薄膜材料和器件的研究。E-mail: wangkx@shanghaitech.edu.cn

Liu Ding-quan (1964—), male, born in Chenggu, Shaanxi Province. Doctor, doctoral supervisor and researcher. Currently he is the director of the research office of optical films, materials and devices, and the distinguished professor of Shanghai University of Science and Technology. His research is focused on the thin film optics and technology, infrared optical thin film and space application, and micro nano optics, etc. E-mail: dqliu@mail.sitp.ac.cn

刘定权(1964—),男,陕西城固人,博士,博士生导师,研究员,现任光学薄膜、材料与器件研究室主任,上海科技大学特聘教授。主要从事薄膜光学与技术、红外光学薄膜及空间应用、微纳光学等方面的科研工作。E-mail: dqliu@mail.sitp.ac.cn

Chen Gang (1983—), male, born in Yinxian County, Zhejiang Province. Doctor and senior engineer. He mainly engages in the design, development and space application of optical films. E-mail: gangchen@mail.sitp.ac.cn

陈 刚(1983—),男,浙江鄞县人,博士,高级工程师,主要从事光学薄膜的设计、研制和空间应用方面的研究工作。E-mail: gangchen@mail.sitp.ac.cn